CHINESE OPTICS LETTERS

Vol. 19, No. 9 | September 2021

Theoretical analysis of periodically poled $LiNbO_3$ nonlinear mirror and its application in a passively mode-locked Nd:YSAG laser

Lina Zhao (赵丽娜)[1,2*], Fangxin Cai (蔡芳馨)[1], Luyang Tong (仝鲁阳)[1], Ye Yuan (袁 野)[1], Wenyu Zhang (张文雨)[1], and Yangjian Cai (蔡阳健)[1,2**]

[1] College of Physics and Electronics, Center of Light Manipulations and Applications, Shandong Normal University, Jinan 250014, China

[2] Shandong Provincial Key Laboratory of Optics and Photonic Device, Jinan 250014, China

*Corresponding author: lnzhao@sdnu.edu.cn

**Corresponding author: yangjiancai@suda.edu.cn

Received November 23, 2020 | Accepted March 4, 2021 | Posted Online June 4, 2021

In this paper, we report a passively mode-locked Nd:$Y_3Sc_2Al_3O_{12}$ (Nd:YSAG) laser using a periodically poled $LiNbO_3$ (PPLN) superlattice. Nonlinear mirror mode locking based on PPLN intracavity frequency doubling was theoretically analyzed. The modulation depth of nonlinear reflectivity of the nonlinear mirror is approximately 8.8%. Optical performances of the mode-locked laser including output power, radio frequency spectrum, and optical spectrum were experimentally investigated. An average output power of 710 mW with a slope efficiency of 14.6% was obtained at the pump power of 6.5 W. The repetition rate is 101.7 MHz, and the signal-to-noise ratio of the mode-locked pulse is 45 dB. The mode-locked pulse width was approximately 9 ps.

Keywords: Nd:YSAG; periodically poled $LiNbO_3$ superlattice; passively mode-locked laser.

DOI: 10.3788/COL202119.091403

1. Introduction

All-solid-state passively mode-locked lasers have received wide attention due to their broad applications in industrial processing, spectroscopy, and medicine[1–4]. In passively mode-locked lasers, ultrafast pulses are mostly produced by using intracavity saturable absorbers (SAs), such as a semiconductor SA mirror (SESAM)[5], carbon nanotubes[6], graphene oxide SAs[7], and graphene-like two-dimensional (2D) materials[8]. Besides SAs, passive mode locking based on intracavity frequency doubling is a promising method. There are generally two types of mechanisms: frequency doubling nonlinear mirror (NLM) mode locking[9–11] and cascaded second-order nonlinear mode locking (CSM)[12,13]. The NLM is based on the phase-matching method in nonlinear crystals and can provide a low self-starting threshold. The CSM is based on the nonlinear phase shift in phase-mismatched nonlinear crystals, which has a relatively high self-starting threshold. The mechanism of CSM is similar to Kerr lens mode locking. The nonlinear phase shift leads to a nonlinear refractive index, which corresponds to an effective lens with a certain focal length acting like a Kerr lens.

Recently, polycrystalline ceramics as laser gain media have several advantages over conventional single crystals, since they have a prolonged fluorescence lifetime and a broadened fluorescence spectrum[14–19]. Therefore, they could be potentially applied in solid-state lasers for better laser performances, such as ultrashort pulse generation and teraherz generation. Among them, Nd:$Y_3Sc_2Al_3O_{12}$(Nd:YSAG) is a good candidate for ceramic lasers. Passively Q-switched, dual-wavelength passively Q-switched mode-locked (QML), and continuous wave mode-locked (CWML) Nd:YSAG lasers have been researched. In 2007, Sato *et al.* used LiB_3O_5 (LBO) crystals as nonlinear crystals to achieve dual-wavelength CWML at wavelengths of 1061 nm and 1063 nm. The pulse width was 10 ps, and the maximum average output power was 560 mW[17]. In 2017, Feng *et al.* reported a dual-wavelength synchronous mode-locking laser using a SESAM at wavelengths of 1060.8 nm and 1063.2 nm, with a mode-locked pulse width of 3.8 ps and a maximum average output power of 470 mW[15]. Gao *et al.* reported a dual-wavelength QML laser at 1058.97 nm and 1061.49 nm using black phosphorus (BP) as an SA, and the maximum output power was 177.3 mW[16]. In 2020, Zhang *et al.* demonstrated a passively Q-switched laser using a ReS_2 nanosheet as an SA at the wavelength of 1061 nm, and the maximum average output power was 356 mW[18].

Compared with the SA, the advantage of mode-locking based on intracavity frequency doubling is that it has higher damage threshold and output power. The periodically poled $LiNbO_3$ (PPLN) superlattice based on quasi-phase-matching is suitable for mode locking due to its relatively high nonlinear coefficient d_{eff} and no walk-off effect. Several research groups have demonstrated mode locking with periodically poled superlattices. In 2005, Holmgren *et al.* reported the mode-locked $Nd:GdVO_4$ laser using periodically poled $KTiOPO_4$ (PPKTP). The mode-locked pulse width is 2.8 ps, and the spectral bandwidth is 0.6 nm[20]. In 2011, Liu *et al.* demonstrated the 1342 nm mode-locked $Nd:YVO_4$ laser using PPLN as a nonlinear crystal. The mode-locked pulse duration is 9.5 ps, and the spectral bandwidth is 0.34 nm[10]. In 2020, our group reported the mode-locked $Nd:Gd_{3x}Y_{3(1-x)}Sc_2Ga_{3(1+\delta)}O_{12}$ ($x = 0-1, \delta = -0.2-0.2$) (Nd:GYSGG) laser using PPLN[21]. Compared with them, the Nd:YSAG laser has a wider spectrum, and the theoretical pulse duration will be shorter. Furthermore, theoretical analysis on the NLM as an effective SA and its performances in Nd:YSAG lasers have not been reported. In this Letter, we report on the NLM mode-locked Nd:YSAG laser with PPLN, where the spectral bandwidth is 1.6 nm, and the average output power is 710 mW. The NLM mode locking was theoretically analyzed. CW and CWML performances were investigated. The average output powers of CW and CWML lasers were 930 and 710 mW, respectively. The repetition rate was 101.7 MHz.

2. Theoretical Analysis

The NLM contains a PPLN superlattice as a nonlinear crystal and an output coupler (OC), which has partial reflectivity for the fundamental wave (FW) and high reflectivity for the second harmonic (SH), as shown in Fig. 1(a). The extended nonlinear Schrodinger equation (NLSE) including the effects of dispersion and Kerr nonlinearity is used to analyze to performance of the NLM. In the slowly varying envelope approximation and in absence of diffraction, the NLSE of the FW and SH can be described as follows[22]:

$$\begin{aligned}
&\frac{\partial A_F}{\partial z} - j\frac{\beta_{2F}}{2}\frac{\partial^2 A_F}{\partial T^2} - \frac{\beta_{3F}}{6}\frac{\partial^3 A_F}{\partial T^3} \\
&\quad = -j\frac{\omega_F d_{\text{eff}}}{n_F c} A_s A_F^{\star} \exp(-j\Delta k \cdot z) - j\frac{\omega_F n_{2F}}{cA_{\text{eff}}}|A_F|^2 A_F \\
&\frac{\partial A_s}{\partial z} + (\beta_{1s} - \beta_{1F})\frac{\partial A_s}{\partial T} - j\frac{\beta_{2s}}{2}\frac{\partial^2 A_s}{\partial T^2} - \frac{\beta_{3s}}{6}\frac{\partial^3 A_s}{\partial T^3} \\
&\quad = -j\frac{\omega_s d_{\text{eff}}}{2n_s c} A_F A_F \exp(j\Delta k \cdot z) - j\frac{\omega_s n_{2s}}{cA_{\text{eff}}}|A_s|^2 A_s,
\end{aligned} \tag{1}$$

where A_m is the electric field envelope ($m = F, s$, representing FW and SH); β_{1m} is the inverse of group velocity; β_{2m} is the second-order group velocity dispersion; β_{3m} is the third-order group velocity dispersion; ω_m is the center frequency; n_m is the refractive index; d_{eff} is the effective nonlinear coefficient of PPLN; Δk is the phase mismatch; z is the longitudinal position in the crystal; n_{2m} is the nonlinear refractive index; A_{eff} is the effective area in PPLN. For the first equation, the second and third items on the left side are related to second-order and third-order dispersion of the FW, respectively. For the second equation, the second, third, and fourth items on the left side are related to group velocity mismatch (GVM) and second-order and third-order dispersion of the SH wave, respectively. On the right side, the two expressions are nonlinear coupled-wave items and self-phase modulation. After doubly passing PPLN, the nonlinear reflectivity of the FW is defined as $R_{\text{NL}} = I_{\text{Fr}}/I_{\text{Fi}}$, where I_{Fi}, I_{Fr} are the incident and reflective light intensity of the FW. In our simulation, the reflectivity of the OC for the FW is 91%, and phase mismatch $\Delta k = 0$. Figure 1(b) shows the nonlinear reflectivity of the NLM dependence on the intracavity power. With the increase of intracavity power, the reflectivity of the FW increases nonlinearly and becomes saturated under relatively high intracavity power. The performance of the NLM is like an effective SA, leading to mode locking. Thus, the curve could be fitted with the saturable absorption formula,

$$R_n(I) = 1 - \Delta D \times \exp(-I/I_{\text{sat}}) - \alpha_{\text{ns}}. \tag{2}$$

Here, R_n is the nonlinear reflection, ΔD is the modulation depth, I is the incident intensity, I_{sat} is the saturable intensity, and α_{ns} is the nonsaturable loss. The nonlinear coupled-wave item in Eq. (1) plays an important role when the NLM acts as an effective SA. As shown in Fig. 1(b), nonlinear reflectivity varies when d_{eff} is set to have different values. At higher d_{eff},

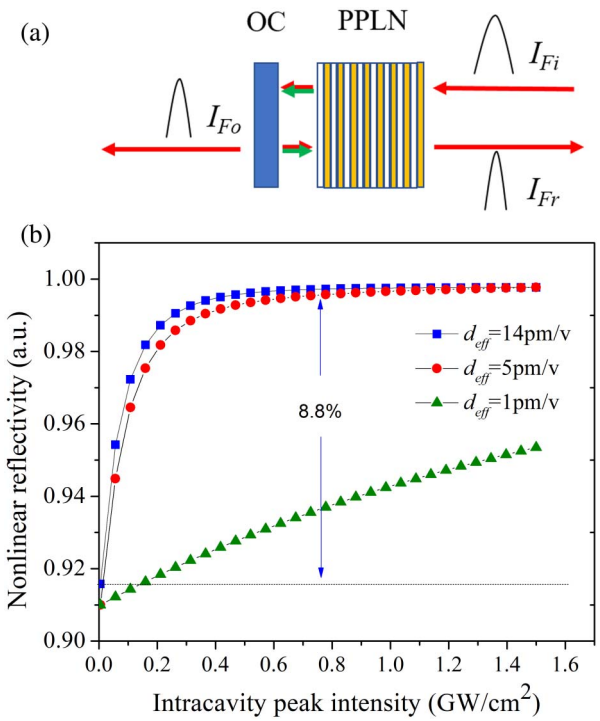

Fig. 1. (a) Diagram of nonlinear mirror. (b) Nonlinear reflectivity dependence on intracavity peak intensity.

Table 1. Modulation Depth, Saturable Intensity, and Nonsaturable Loss Dependence on Effective Nonlinear Coefficient.

d_{eff}(pm/V)	ΔD	I_{sat}(GW/cm^2)	α_{ns}
14	8.8%	0.091	0.3%
5	8.7%	0.113	0.4%
1	7.6%	1.800	1.5%

the effective SA is prone to be saturated at lower intracavity intensity. On the other hand, if the superlattice is of poor poling quality, it leads to lower d_{eff}, and NLM mode locking will have a relatively high self-starting threshold. After fitting the curves using Eq. (2), the modulation depth, saturable intensity, and nonsaturable loss were shown in Table 1. The modulation depth decreases, but saturable intensity and nonsaturable loss increase with decreasing d_{eff}. The increasing saturable intensity indicates that the MLN mode locking will have a high threshold. It is worth noting that the modulation depth, saturable intensity, and nonsaturable loss are 8.8%, 91 MW/cm^2, and 0.3%, respectively, when d_{eff} is set to be 14 pm/V, which corresponds to perfect poling of the superlattice with a duty cycle of 1:1.

3. Material and Methods

The mode-locking performance of the Nd:YSAG laser was investigated by using a standard Z-type cavity in the experiment. Figure 2 shows the diagram of the experimental setup of the mode-locked laser. The length, width, and height of the Nd:YSAG crystal was 8 mm × 4 mm × 4 mm. It was installed in a copper bracket cooled by water circulation, and the temperature was maintained at 14°C. A fiber-coupled diode laser delivered 30 W pump light, and the central emission wavelength was 808 nm. An optical coupling system was utilized to yield a beam the same as a pump beam onto the laser crystal, where the beam radius is 200 μm. M1 was a flat mirror with an antireflection (AR) coating ($T > 98\%$) at 808 nm and a highly reflective coating ($R > 99.5\%$) at 1.06 μm. M2 (radius of curvature: 500 mm) and M3 (radius of curvature: 200 mm) were plane-concave mirrors. Both of them were coated with high reflectivity ($R > 99\%$) at 1030–1080 nm. The OC M4 was a dichroic mirror that had partial reflectivity ($R = 91\%$) for FW and high reflectivity for the SH. The length of the PPLN superlattice was 5 mm. The period of the PPLN was 6.92 μm. In the experiment, the PPLN crystal was put in an oven, and the oven was located near the OC M4. In order to obtain a linearly polarized output beam, we inserted a Brewster polarization plate between the plane-concave mirrors M2 and M3. The total length of the resonant cavity was about 1.45 m. We calculated that the beam radii on the Nd:YSAG crystal and PPLN crystal were 190 μm and 80 μm, respectively.

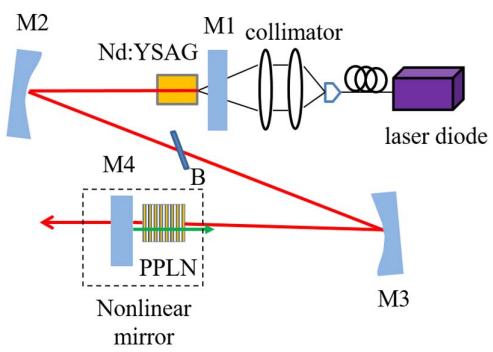

Fig. 2. Diagram of mode-locked Nd:YSAG laser (M1, flat mirror; M2, M3, plane-concave mirror; M4, output coupler; B, Brewster polarization plate; dotted rectangle is nonlinear mirror).

4. Experimental Results and Discussion

First, the PPLN was not inserted into the cavity, and the characteristics of the CW laser were studied. The pump power threshold was 1.5 W, and the output power increased linearly as the pump power increased. As shown in Fig. 3, the output average power reaches 930 mW when the pump power increases to 6.5 W. The corresponding slope efficiency is 18.3%.

Then, the PPLN was inserted into the resonant cavity to study the performance of the CWML. The FW would be converted into SH by frequency doubling when it propagated through the PPLN. In order to improve the SH conversion efficiency, the temperature of the PPLN crystal was adjusted to achieve a phase-matching point. The optimized temperature for frequency doubling was controlled at about 20°C. As shown in Fig. 3, CW mode locking occurs when the pump power increased to 5 W. The cavity delivered 710 mW average output power with a slope efficiency of 14.6 % under the pump power of 6.5 W.

The pulse sequence was detected by a Si detector (Thorlabs, DET025AFC). The interval between adjacent pulses was 9.8 ns, which was in good agreement with the calculated roundtrip time by using a cavity length of 1.45 m, as shown in Fig. 4(a).

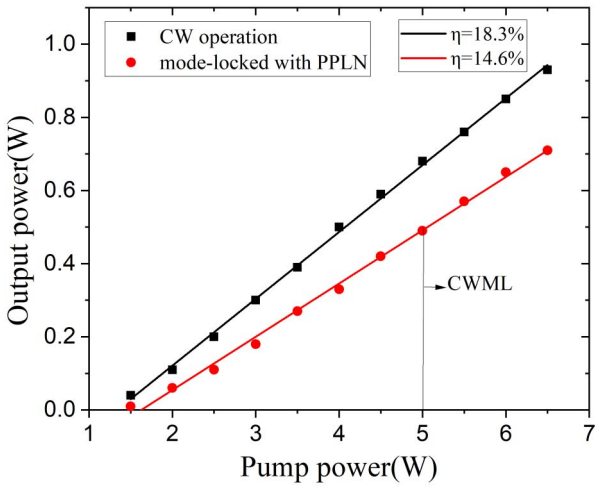

Fig. 3. Average output power dependence on pump power in the CW and CWML regime.

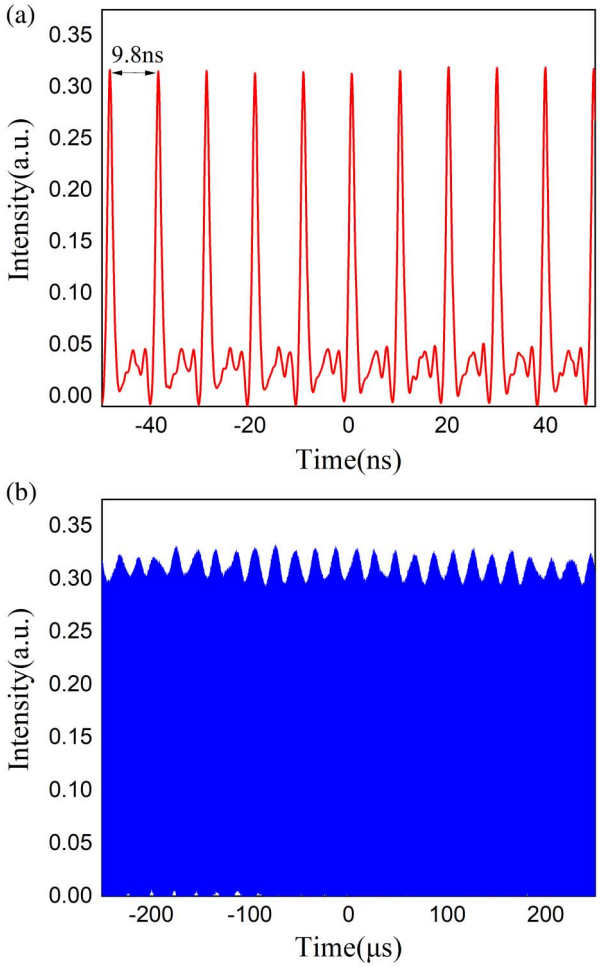

Fig. 4. (a) Mode-locked pulse sequence at 100 ns time scale. (b) Mode-locked pulse sequence at 500 μs time scale.

Figure 4(b) shows the pulse sequence trace at 500 μs time scale. A digital oscilloscope (LeCroy, HDO4104A), which had a spectrum analyzing function, was used to measure radio frequency (RF) waveform, as shown in Fig. 5. The resolution bandwidth (RBW) was set to be 2 kHz within a span of 3.5 MHz. The fundamental central frequency was 101.7 MHz. The signal-to-noise ratio of the pulse was 45 dB. An optical spectrum analyzer (Avantes, AVASPEC-3648-USB2) was used to measure the optical spectrum. As shown in Fig. 6, there are two peaks oscillating in the cavity, 1061 nm and 1063.5 nm, respectively. To determine which wavelength participates in the mode-locking process, we made the analysis as follows:

$$\Delta k = k_2 - 2k_1 - G, \tag{3}$$

where k_1, k_2 are the wave vectors of the FW and SH. G is the reciprocal vector of the PPLN, and $G = \frac{2\pi}{\Lambda}$, where Λ is the period of the PPLN. In our experiment, under the oven temperature of 20°C, the phase-matching condition was satisfied at 1061 nm, as shown in Fig. 7. Therefore, the wavelength at 1061 nm was determined to participate in frequency doubling NLM mode locking. However, frequency doubling at 1063.5 nm was phase

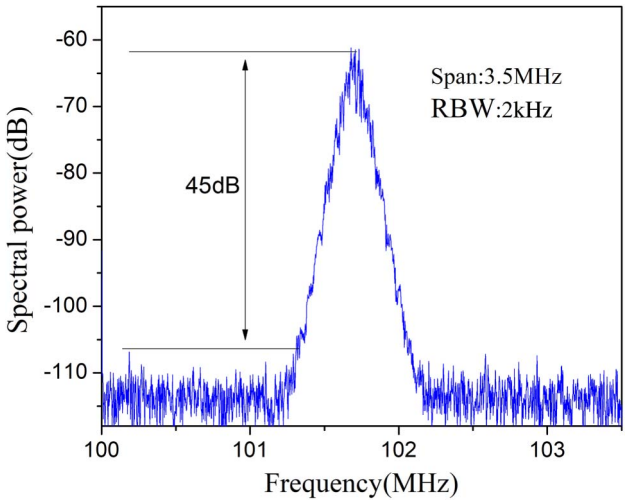

Fig. 5. Radio frequency waveform of CWML laser.

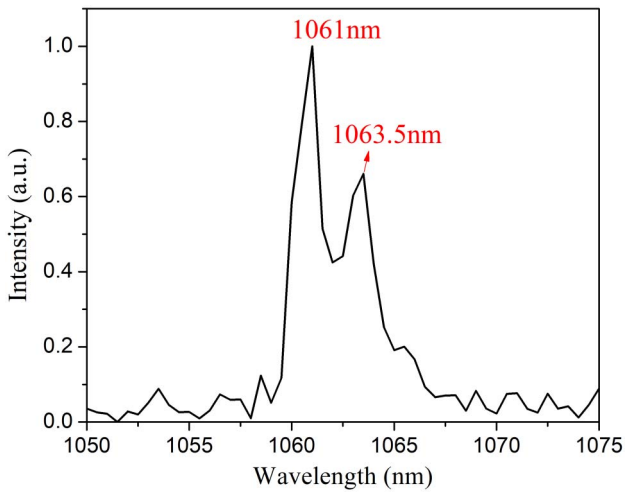

Fig. 6. Optical spectrum of mode-locked Nd:YSAG laser.

mismatched, which did not take part in the CSM, since CSM is Kerr-lens-like mode locking. The reason is that, in our setup, the cavity mode radius in Nd:YSAG is 190 μm, and the pump beam radius is 200 μm, so the cavity mode is smaller than that of the pump beam, and it cannot satisfy the condition of Kerr-lens mode locking. Moreover, 1063.5 nm also did not take part in NLM mode-locking, because frequency doubling at 1063.5 nm was phase mismatched, thus there is no efficient frequency conversion, and mode locking could not start.

The mode-locked pulse width can be estimated according to the following method. The full width at half-maximum (FWHM) of the spectrum is 1.6 nm at the central wavelength of 1061 nm. According to the time bandwidth product of a pulse with a Gaussian curve ($\Delta\nu^*\Delta t = 0.44$), we calculated the pulse duration to be 1 ps. However, the pulse will be broadened due to the GVM in the PPLN. The GVM of the FW and SH after passing the PPLN twice is 1.6 ps/mm. In the experiment, the length of PPLN is 5 mm, so the SH is relatively delayed to the

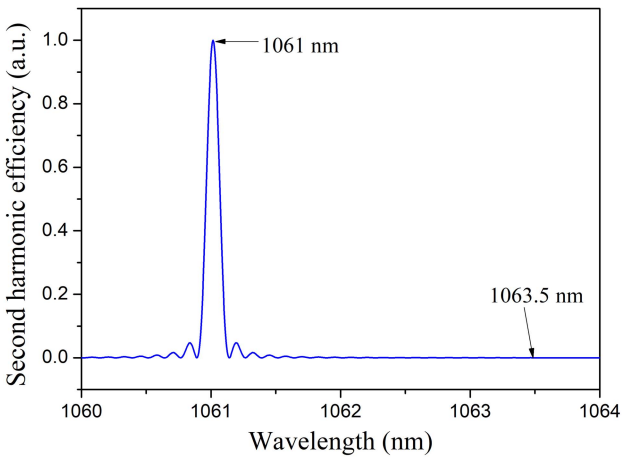

Fig. 7. Second harmonic efficiency at different wavelengths.

FW by 8 ps. Thus, the final minimum pulse width is estimated to be 9 ps.

It is worth noting that the minimum pulse intensity of the intracavity pulse is 121 MW/cm^2, assuming that the conversion of SH generation is a small signal approximation. It is higher than the theoretical saturation intensity of 91 MW/cm^2, which corresponds to a maximum d_{eff} of 14 pm/V. Therefore, it indicates that the PPLN superlattice is of high poling quality, and the NLM could effectively act as an SA in our experiment.

5. Conclusions

In conclusion, we report a passively mode-locked Nd:YSAG laser based on a PPLN superlattice NLM. NLM mode locking was theoretically analyzed. The modulation depth of nonlinear reflectivity of the NLM was approximately 8.8%. Optical performances of the mode-locked laser including output power, RF spectrum, and optical spectrum were experimentally investigated. An average output power of 710 mW with a slope efficiency of 14.6% was obtained at the pump power of 6.5 W. The repetition rate was 101.7 MHz, and the signal-to-noise ratio of the mode-locked pulse was 45 dB. The mode-locked pulse width was approximately 9 ps.

Acknowledgement

This work was supported by the National Key Research and Development Project of China (No. 2019YFA0705000), the National Natural Science Foundation of China (Nos. 91950106, 11404196, 11525418, 91750201, and 11974218), the Innovation Group of Jinan (2018GXRC010), and the Local Science and Technology Development Project of the Central Government (No. YDZX20203700001766).

References

1. I. V. Pechenezhskiy, X. P. Hong, G. D. Nguyen, J. E. P. Dahl, R. M. K. Carlson, F. Wang, and M. F. Crommie, "Infrared spectroscopy of molecular submonolayers on surfaces by infrared scanning tunneling microscopy: tetramantane on Au (111)," Phys. Rev. Lett. **111**, 126101 (2013).
2. J. Baxter, "Optical coherence tomography: tunable for medicine," Nat. Photon. **6**, 70 (2012).
3. C. J. Saraceno, C. Schriber, M. Mangold, M. Hoffmann, O. H. Heckl, C. R. E. Baer, M. Golling, T. Sudmeyer, and U. Keller, "SESAMs for high-power oscillators: design guidelines and damage thresholds," IEEE J. Sel. Top. Quantum Electron. **18**, 29 (2012).
4. M. F. Zhao, Z. M. Zhang, X. Y. Feng, M. Y. Zong, J. Liu, X. D. Xu, and H. Zhang, "High repetition rate passively *Q*-switched laser on Nd:SRA at 1049 nm with MXene $Ti_3C_2T_x$," Chin. Opt. Lett. **18**, 041401 (2020).
5. Y. X. Fan, J. L. He, Y. G. Wang, S. Liu, H. T. Wang, and X. Y. Ma, "2-ps passively mode-locked Nd: YVO_4 laser using an output-coupling-type semiconductor saturable absorber mirror," Appl. Phys. Lett. **86**, 101103 (2005).
6. J. H. Yim, W. B. Cho, S. Lee, Y. H. Ahn, K. Kim, H. Lim, G. Steinmeyer, V. Petrov, U. Griebner, and F. Rotermund, "Fabrication and characterization of ultrafast carbon nanotube saturable absorbers for solid-state laser mode locking near 1 μm," Appl. Phys. Lett. **93**, 161106 (2008).
7. L. Zhang, Y. G. Wang, H. J. Yu, S. B. Zhang, W. Hou, X. C. Lin, and J. M. Li, "High power passively mode-locked Nd:YVO_4 laser using graphene oxide as a saturable absorber," Laser Phys. **21**, 2072 (2011).
8. X. Sun, B. T. Zhang, Y. Li, X. Luo, G. Li, Y. Chen, C. Zhang, and J. L. He, "Tunable ultrafast nonlinear optical properties of graphene/MoS_2 van der Waals heterostructures and their application in solid-state bulk lasers," ACS Nano **12**, 11376 (2018).
9. H. Iliev, I. Buchvarov, S. Kurimura, and V. Petrov, "High-power picosecond Nd:$GdVO_4$ laser mode locked by SHG in periodically poled stoichiometric lithium tantalite," Opt. Lett. **35**, 1016 (2010).
10. Y. H. Liu, Z. D. Xie, S. D. Pan, X. J. Lv, Y. Yuan, X. P. Hu, J. Lu, L. N. Zhao, C. D. Chen, G. Zhao, and S. N. Zhu, "Diode-pumped passively mode-locked Nd:YVO_4 laser at 1342 nm with periodically poled $LiNbO_3$," Opt. Lett. **36**, 698 (2011).
11. L. N. Zhao, L. Y. Tong, F. X. Cai, Y. Yuan, and Y. J. Cai, "Wavelength-tunable nonlinear mirror mode-locked laser based on MgO-doped lithium niobite," Crystals **10**, 861 (2020).
12. H. Cheng, X. D. Jiang, X. P. Hu, M. L. Zhong, X. J. Lv, and S. N. Zhu, "Diode-pumped 1988-nm Tm:YAP laser mode-locked by intracavity second-harmonic generation in periodically poled $LiNbO_3$," Opt. Lett. **39**, 2187 (2014).
13. S. T. Lin and C. H. Huang, "Effects of nonlinear phase in cascaded mode locked Nd:YVO_4 laser," Opt. Express **27**, 504 (2019).
14. Q. Song, G. J. Wang, B. Y. Zhang, Q. L. Zhong, W. J. Wang, M. H. Wang, G. H. Sun, Y. Bo, and Q. J. Peng, "Passively *Q*-switched mode-locked dual-wavelength Nd:GYSGG laser using graphene oxide saturable absorber," Opt. Commun. **347**, 64 (2015).
15. C. Feng, H. N. Zhang, Q. P. Wang, and J. X. Fan, "Dual-wavelength synchronously mode-locked laser of a Nd:$Y_3ScAl_4O_{12}$ disordered crystal," Laser Phys. Lett. **14**, 045804 (2017).
16. C. C. Gao, S. H. Lv, G. Zhu, G. J. Wang, X. C. Su, B. B. Wang, S. Kumar, R. Q. Dou, F. Peng, Q. L. Zhang, H. J. Yu, X. C. Lin, and B. Y. Zhang, "Self-*Q*-switching and passively *Q*-switched mode-locking of dual-wavelength Nd:YSAG laser," Opt. Laser Technol. **122**, 105860 (2020).
17. Y. Sato, J. Saikawa, and T. Taira, "Characteristics of Nd^{3+}-doped $Y_3ScAl_4O_{12}$ ceramic laser," Opt. Mater. **29**, 1277 (2007).
18. N. Zhang, S. K. Zeng, Z. X. Wang, B. X. Li, and Y. H. Pan, "Nd:YSAG *Q*-switched laser with anisotropic ReS_2 nanosheets," Optik **208**, 164542 (2020).
19. J. L. Wang, K. Q. Zhao, T. Feng, X. L. Zhu, and W. B. Chen, "1.5 J high-beam-quality Nd:LuAG ceramic active mirror laser amplifier," Chin. Opt. Lett. **18**, 021401 (2020).
20. S. J. Holmgren, V. Pasiskevicius, and F. Laurell, "Generation of 2.8 ps pulses by mode-locking a Nd:$GdVO_4$ laser with defocusing cascaded Kerr lensing in periodically poled KTP," Opt. Express **13**, 5270 (2005).
21. F. X. Cai, L. Y. Tong, Y. Yuan, Y. G. Cai, and L. N. Zhao, "Diode-pumped passively mode-locked Nd:GYSGG laser at 1061 nm with periodically poled $LiNbO_3$ nonlinear mirror," J. Mod. Opt. **67**, 552 (2020).
22. F. Saltarelli, A. Diebold, I. J. Graumann, C. R. Phillips, and U. Keller, "Modelocking of a thin-disk laser with the frequency-doubling nonlinear-mirror technique," Opt. Express **25**, 23254 (2017).